© 2016. Published by The Company of Biologists Ltd | Journal of Cell Science (2016) 129, 2625-2637 doi:10.1242/jcs.173708

RESEARCH ARTICLE

NECAP2 controls clathrin coat recruitment to early endosomes for fast endocytic recycling

John P. Chamberland, Lauren T. Antonow, Michel Dias Santos and Brigitte Ritter*

ABSTRACT

Endocytic recycling returns receptors to the plasma membrane following internalization and is essential to maintain receptor levels on the cell surface, re-sensitize cells to extracellular ligands and for continued nutrient uptake. Yet, the protein machineries and mechanisms that drive endocytic recycling remain ill-defined. Here, we establish that NECAP2 regulates the endocytic recycling of EGFR and transferrin receptor. Our analysis of the recycling dynamics revealed that NECAP2 functions in the fast recycling pathway that directly returns cargo from early endosomes to the cell surface. In contrast, NECAP2 does not regulate the clathrin-mediated endocytosis of these cargos, the degradation of EGFR or the recycling of transferrin along the slow, Rab11-dependent recycling pathway. We show that protein knockdown of NECAP2 leads to enlarged early endosomes and causes the loss of the clathrin adapter AP-1 from the organelle. Through structure-function analysis, we define the protein-binding interfaces in NECAP2 that are crucial for AP-1 recruitment to early endosomes. Together, our data identify NECAP2 as a pathway-specific regulator of clathrin coat formation on early endosomes for fast endocytic recycling.

KEY WORDS: EGFR, Rab4, Clathrin, Early endosomes, Endosomal sorting, Fast recycling

INTRODUCTION

Receptor levels at the cell surface are dynamically regulated to control numerous cellular functions, including receptor signaling, nutrient uptake and cell migration. To remove membrane-bound molecules and receptor–ligand complexes from the surface, these cargos are internalized through clathrin-mediated and clathrin-independent endocytosis. Internalized receptors then enter early endosomes, which function as the key sorting station in deciding the fate of receptor cargo. Ubiquitylated receptors engage the ESCRT complex for sorting into multivesicular bodies and subsequent receptor degradation (Raiborg and Stenmark, 2009). The degradative pathway is crucial for the termination of signaling cascades downstream of ligand-activated receptor tyrosine kinases, such as epidermal growth factor receptor (EGFR). In contrast, endocytic recycling returns receptors to the cell surface, thereby replenishing the surface pool of receptors to re-sensitize cells to extracellular ligands, to maintain nutrient supply and to promote cell motility (Grant and Donaldson, 2009; Kelly and Owen, 2011; Maritzen et al., 2015).

Boston University School of Medicine, Biochemistry Department, Boston, MA 02118, USA.

*Author for correspondence (britter@bu.edu)

J.P.C., 0000-0002-7862-1371; L.T.A., 0000-0002-9622-4994; M.D.S., 0000-0002-5976-7973; B.R., 0000-0002-0094-0460

Received 28 April 2015; Accepted 19 May 2016

Early endosomal sorting and endocytic recycling are regulated by members of the Arf and Rab families of small GTPases. Activation of Rabs and Arfs by guanine-nucleotide exchange factors (GEFs) enables the GTP-bound GTPases to recruit downstream effector proteins that fulfill pathway-specific functions and promote the formation of cargo-carrying vesicles and tubules. For example, Rab35 mediates cadherin recycling, whereas Arf6 controls β1-integrin recycling (Allaire et al., 2013). Transferrin receptor (TfnR) is the canonical marker of endocytic recycling, and transferrin remains bound to the receptor until TfnR reaches the cell surface. Notably, TfnR enters into recycling pathways with differential kinetics (Sheff et al., 1999). The fast recycling pathway directly returns TfnR from early endosomes to the cell surface and is regulated by Rab4a (van der Sluijs et al., 1992). In the slow recycling pathway, Rab4b-mediated sorting sends TfnR from early to Rab11a-positive recycling endosomes for subsequent transport to the cell surface (Bhuin and Roy, 2015; Perrin et al., 2013; Welz et al., 2014).

The fast and slow recycling pathways both recruit the clathrin adapter complex AP-1 and clathrin, albeit through different mechanisms. Rab4b directly recruits AP-1 as an effector to promote cargo sorting from early to recycling endosomes (Perrin et al., 2013). Rab4a instead triggers a multistep GTPase cascade that, in addition to AP-1, also recruits the clathrin adapters AP-3 and GGA3 to early endosomes (D'Souza et al., 2014). It is currently unclear whether the variety of clathrin adapters recruited by Rab4a represents a functional diversity in Rab4a-mediated recycling. However, the formation of recycling vesicles and tubules are likely to require a larger protein machinery beyond the clathrin adapters and clathrin themselves, similar to the complexity seen for clathrin-mediated endocytosis (Kirchhausen et al., 2014; McMahon and Boucrot, 2011). The characterization of the protein machineries driving endocytic recycling will be crucial for the understanding of the functional divergence between different recycling pathways and their role in normal cell function.

We have previously identified the adaptin ear-binding coat-associated protein (NECAP) family during our proteomics analysis of clathrin-coated vesicles from adult rat brain (Blondeau et al., 2004; Ritter et al., 2003). The two members of the family, NECAP1 and NECAP2, share a high degree of sequence and structural similarity. At their N-terminus, the NECAPs encode a pleckstrin homology (PH)-like domain that functions as a protein-binding module (Ritter et al., 2007). In addition, NECAPs display peptide motifs at their C-terminus that promote interactions with the clathrin adaptor complexes AP-1 and AP-2 (Ritter et al., 2004). Our functional studies of NECAP1 have revealed that NECAP1 functions together with AP-2 in clathrin-mediated endocytosis at the cell surface (Ritter et al., 2013). In fact, the NECAP1 PH domain binds to some of the same accessory proteins that interact with AP-2 such that NECAP1 and AP-2 cooperate in the recruitment of accessory proteins to the site of vesicle formation (Ritter et al.,

Journal of Cell Science (2016) 129, 2625-2637 doi:10.1242/jcs.173708

2013). NECAP1 depletion interferes with normal clathrin-mediated endocytosis, altering the number and size of forming vesicles and impairing clathrin-mediated internalization of ligand-bound EGFR (Ritter et al., 2013).

Notably, NECAP2 does not rescue the NECAP1 knockdown phenotype (Ritter et al., 2013), indicating that the two proteins are functionally divergent. Here, we provide the first functional characterization of NECAP2 and establish a role for NECAP2 in the fast recycling pathway. We demonstrate that NECAP2 is essential for the recruitment of AP-1 to early endosomes and for the efficient recycling of EGFR and TfnR. Taken together, our results identify NECAP2 as a central component of the protein machinery for fast recycling.

RESULTS

The Human Protein Atlas indicates a broad protein expression pattern of NECAP2, with higher levels in several tissues, including breast, kidney and lung. We thus decided to use protein knockdown (KD) in MCF10A cells, which are adherent normal breast epithelial cells, as well as in the commonly used cell lines HeLa and COS-7 to define the function of NECAP2.

NECAP2 does not regulate the size and number of endocytic clathrin-coated pits

To test whether NECAP2 depletion causes changes in the number and size of endocytic clathrin-coated pits and vesicles, similar to NECAP1 knockdown (Ritter et al., 2013), we labeled these structures by using the α-adaptin subunit of the endocytosis-specific clathrin adapter AP-2 in control cells and cells depleted of NECAP1 or NECAP2 (Fig. 1A,B). The immunofluorescence signal intensity of the coat proteins AP-2 and clathrin directly correlates to the size of the forming structure (Antonescu et al., 2011; Ehrlich et al., 2004; Mettlen et al., 2010; Ritter et al., 2013). As expected, NECAP1 knockdown decreased the number and increased the intensity of AP-2-labeled puncta, whereas NECAP2 depletion has no effect (Fig. 1B–D). Thus, in contrast to NECAP1, NECAP2 is not required for the control of the number and size of clathrin-coated pits and vesicles at the plasma membrane.

NECAP2 does not affect clathrin-mediated endocytosis

We next sought to test for changes in clathrin-mediated endocytosis. TfnR is constitutively internalized through clathrin-mediated endocytosis and recycles to the plasma membrane through both the fast and slow recycling pathways. By using fluorescence imaging, we first quantified the amount of fluorescently labeled transferrin internalized into MCF10A and HeLa cells within 1 min. This timeframe ensures analysis of endocytic events and excludes potential secondary effects due to changes in transferrin and TfnR recycling. These assays revealed no differences in transferrin uptake between control, NECAP1 KD and NECAP2 KD cells (Fig. 1E–H). To verify these results under different experimental conditions, we labeled the surface pool of TfnR by incubating COS-7 cells with Alexa-Fluor-647-labeled transferrin on ice and then shifted the cells to 37°C for 1 or 4 min. After removal of residual transferrin from the cell surface by acid washing, cells were lysed and total protein extracts were separated by SDS-PAGE for quantification of internalized Alexa-Fluor-647-transferrin by quantitative infrared fluorescence measurement using an Odyssey Imaging System (LI-COR Biosciences). These assays confirmed that depletion of NECAP1 or NECAP2 does not affect the rate of transferrin internalization at the purely endocytic 1-min time point (Fig. 1I,J). Interestingly, NECAP2 knockdown resulted in increased transferrin levels at the 4-min time point compared to that in control and NECAP1 KD cells (Fig. 1I,J), suggesting a role of NECAP2 in the sorting of transferrin subsequent to internalization.

We have previously shown that NECAP1 knockdown does not affect transferrin internalization, which is consistent with the data presented here, but that it decreases the clathrin-mediated endocytosis of ligand-bound EGFR in COS-7 cells (Ritter et al., 2013). To test whether NECAP2 plays a role in EGFR internalization, we incubated COS-7 cells on ice with fluorescently labeled EGF and then shifted the cells to 37°C for 2.5 min to allow internalization, followed by removal of residual EGF from the cell surface by acid washing. The amount of surface-bound and internalized EGF was then quantified by performing fluorescence microscopy. These assays revealed differential effects of NECAP1 and NECAP2 on EGFR surface levels and internalization. NECAP1 knockdown did not alter EGFR surface levels but impaired EGF internalization (Fig. 1K–M), consistent with our previous results. In contrast, NECAP2 KD cells displayed lower levels of EGFR on the surface (Fig. 1K,L), even though total EGFR expression levels were comparable to those of control cells (Fig. 2C,D), suggesting that NECAP2 knockdown leads to a redistribution of EGFR within the cell. However, the percentage of surface EGFR internalized in NECAP2 KD cells was comparable to that of control cells (Fig. 1M). Together with the lack of any effect on transferrin internalization, these results demonstrate that NECAP2 does not control clathrin-mediated endocytosis of TfnR and EGFR.

NECAP2 depletion leads to enlarged early endosomes

By using immunofluorescence analysis of endogenous markers, we discovered that NECAP2 knockdown caused a significant increase in the size of early endosomes (Fig. 2A,B). However, NECAP2 knockdown did not alter EEA1 expression levels or the total number of early endosomes per cell (Fig. 2C–E). Binning of early endosomes by size confirmed the prevalence of enlarged early endosomes due to NECAP2 depletion (Fig. 2F,G). Notably, we also observed similar changes in early endosomal morphology in COS-7 and HeLa cells following NECAP2 knockdown (Fig. 2H,I), indicating a general role for NECAP2 in the regulation of early endosomes. In contrast, NECAP1 knockdown had no effect on early endosomal morphology (Fig. 2A,B,E–G), confirming that NECAP1 and NECAP2 serve distinct cellular functions.

Early endosomes receive endocytosed material from clathrin-dependent and -independent pathways and sort cargo for recycling to the cell surface, retrograde transport to the Golgi or degradation in lysosomes. Thus, larger endosomes might be the result of enhanced endocytic influx and/or a decrease in the rate of cargo recycling and/or degradation. Because clathrin-mediated endocytosis is the main endocytic pathway in eukaryotic cells (Bitsikas et al., 2014), and because NECAP2 depletion does not change the number of endocytic clathrin-coated pits (Fig. 1B–D) or the rate of clathrin-dependent internalization (Fig. 1E–M), it is unlikely that changes in the endocytic potential contribute to the morphological changes of early endosomes in NECAP2 KD cells.

NECAP2 controls EGFR cell surface levels and recycling

Following internalization, EGFR enters early endosomes and either recycles back to the cell surface or enters into the degradative pathway. Because our EGF internalization assays indicated that NECAP2 regulates EGFR distribution within cells (Fig. 1K–M), we sought to further define the effects of NECAP2 knockdown on EGFR surface levels, localization and sorting. Labeling the cell

Journal of Cell Science

Journal of Cell Science (2016) 129, 2625-2637 doi:10.1242/jcs.173708

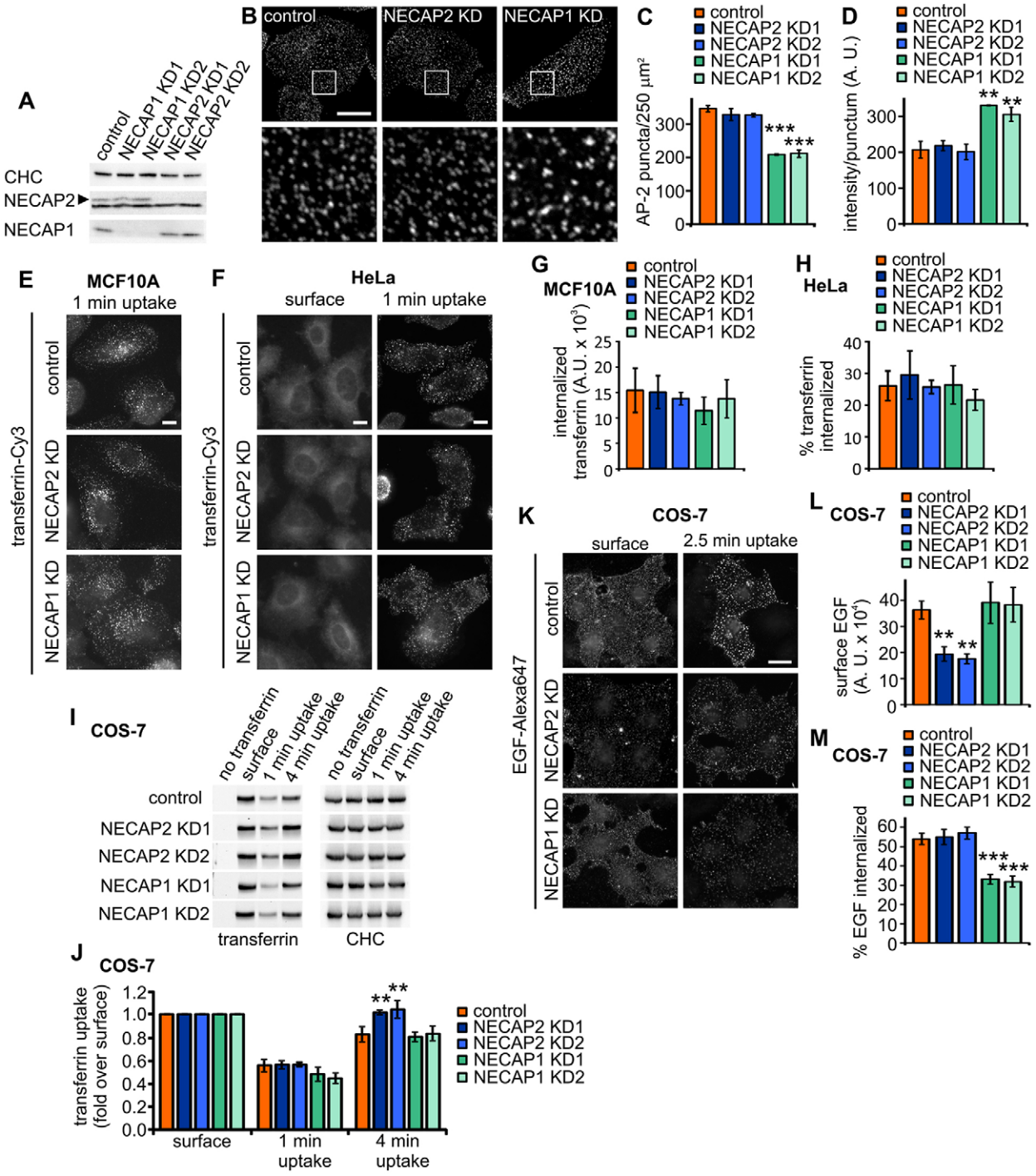

Fig. 1. See next page for legend.

surface pool of EGFR with an antibody directed against the extracellular region of the receptor revealed that NECAP2 knockdown led to a 40% reduction in the surface levels of EGFR at steady-state (Fig. 3A,B), consistent with the decreased levels of surface-bound EGF seen in NECAP2 KD cells (Fig. 1K,L). Because western blot analysis of total protein lysates from control and NECAP2 KD cells showed that NECAP2 depletion does not alter EGFR expression levels (Fig. 2C,D), we used co-immunofluorescence analyses to determine the distribution of EGFR within cells. These studies revealed that at steady-state, EGFR accumulates in EEA1-positive endosomes upon NECAP2 depletion (Fig. 3C,D), suggesting that NECAP2 is required for efficient early endosomal sorting of EGFR.

From early endosomes, EGFR is either recycled to the cell surface or sent for degradation; we thus sought to test for a role of NECAP2 in either sorting pathway. We first tested for changes in EGFR recycling after treatment with TGFα, which leads specifically to EGFR recycling after the ligand dissociates from the receptor in early endosomes (Henriksen et al., 2013; Roepstorff et al., 2009). Control and NECAP2 KD cells were incubated with 10 nM TGFα for 5 min to trigger a wave of EGFR internalization, acid-washed on ice and then chased for 3 or 5 min

Journal of Cell Science (2016) 129, 2625-2637 doi:10.1242/jcs.173708

Fig. 1. NECAP2 is not required for clathrin-mediated endocytosis. (A) Western blot analysis of NECAP2 and NECAP1 expression levels in total protein lysates of control, NECAP2 KD and NECAP1 KD cells. For each protein, KD1 and KD2 refer to two independent siRNAs (see Materials and Methods). The arrowhead indicates the NECAP2-specific band. Clathrin heavy chain (CHC) was used as loading control. (B) Confocal images of the immunofluorescence analysis of the α-adaptin subunit of the endogenous AP-2 expression in control, NECAP2 KD and NECAP1 KD cells as indicated. Scale bar: 15 µm (low magnification images, top row); 3 µm (high magnification images, bottom row). Boxes indicated in the top row show regions of interest magnified in the bottom row. (C,D) Quantification of the number of AP-2 puncta per 250 μm^2 (C) and fluorescence intensity per AP-2 punctum (D); mean±s.e.m., *N*=3 experiments, *n*=17 cells total per condition. A.U., arbitrary units. Statistical analysis using one-way ANOVA followed by Dunnett's post-test revealed significant differences between control and KD cells for C,D, $^{**}P<0.01$, $^{***}P<0.001$. (E,F) Fluorescence analysis after 1 min of transferrin–Cy3 uptake in control, NECAP2 KD and NECAP1 KD cells for MCF10A (E) and HeLa cells (F). (G) Quantification of data shown in E; mean±s.e.m., *N*=3 experiments, *n*=35–55 cells total per group. A.U., arbitrary units. (H) Quantification of the data shown in F as a ratio of the intensity of internalized transferrin–Cy3 over that at the surface; mean±s.e.m., *N*=3 experiments, *n*=125–142 cells total per group. For G,H, statistical analysis using one-way ANOVA followed by Dunnett's post-tests revealed no significant differences. (I) Quantitative infrared fluorescence measurement analysis of transferrin–Cy3 levels and western blot analysis of clathrin expression levels in total protein lysates of control, NECAP2 KD and NECAP1 KD COS-7 cells. For each group, cells were either left untreated (no transferrin), incubated with transferrin–Cy3 on ice to label the TfnR surface pool (surface), or surface-labeled followed by transferrin internalization for 1 or 4 min at 37°C as indicated. CHC, clathrin heavy chain. (J) Quantification of data shown in I; mean±s.e.m., *N*=3 experiments. Statistical analysis using repeated-measures two-way ANOVA followed by Bonferroni post-test revealed no differences at the 1-min time point or between control and NECAP1 KD cells at the 4-min time point, and significant differences were found between control and NECAP2 KD cells at the 4-min uptake time point, $^{**}P<0.01$. (K) Fluorescence analysis of EGF levels on the cell surface and levels internalized within 2.5 min in control, NECAP2 KD and NECAP1 KD COS-7 cells using 2 ng/ml EGF–Alexa-Fluor-647. Scale bar: 20 µm. (L) Quantification of fluorescence intensity of EGF–Alexa-Fluor-647 on the cell surface; mean±s.e.m., *N*=3 experiments, *n*=75–103 cells per group. A.U., arbitrary units. (M) Quantification of the fraction of surface EGF–Alexa-Fluor-647 internalized within 2.5 min, *N*=3 experiments, *n*=114–155 cells per group. For L,M, statistical analysis using repeated-measures one-way ANOVA followed by Dunnett's post-tests revealed significant differences

to allow for EGFR recycling. For each time point, cells were incubated on ice with an EGFR antibody directed against the extracellular region to label the surface pool of EGFR, washed and lysed, and the fraction of antibody-bound EGFR was isolated by immunoprecipitation and detected by western blotting. These studies showed that the 3 min chase did not allow for efficient EGFR recycling in control or NECAP2 KD cells because the receptor surface levels stayed at levels comparable to those remaining on the cell surface after the 5 min TGFα pulse (Fig. 3E,F). Because the rate of exocytosis from early endosomes varies from one to several minutes depending on the cell line, cargo and method of analysis used (Hao and Maxfield, 2000; Sheff et al., 1999, 2002), the vesicles and/or tubules that recycle EGFR from early endosomes might have not yet reached the cell surface after the 3 min chase. Alternatively, recycling might be slightly delayed in our experimental design owing to the incubation on ice prior to the chase that is required to remove residual TGFα from the cell surface after the pulse. However, during the 5 min chase, control cells efficiently recycled EGFR to the cell surface (Fig. 3E,F). In contrast, EGFR surface levels in NECAP2 KD cells remained close to the level that was detected at the end of the TGFα pulse (Fig. 3E,F), demonstrating that NECAP2 knockdown impairs fast EGFR recycling. Consistently, we detected an increase in the number of EGFR-containing EEA1-positive endosomes in NECAP2 KD cells compared to control in response to treatment with 1.5 ng/ml EGF for 3 min (Fig. 3G), although this increase did not reach significance owing to variability between experiments.

NECAP2 is dispensable for EGFR degradation

To determine whether NECAP2 knockdown also alters EGFR degradation, we tested for changes in total EGFR levels over time following ligand-induced internalization. Continuous stimulation with 50 ng/ml EGF, which drives EGFR into the degradative pathway (French et al., 1994; Kornilova et al., 1996; Sigismund et al., 2008), led to a 50% decrease of total EGFR levels within 1 h (Fig. 3I). Although NECAP2 KD cells appeared to show a slight delay, the rate of EGFR degradation during later time points was comparable between control and NECAP2 KD cells, and we did not find a significant difference in the rate of EGFR degradation (Fig. 3H). We next tested whether NECAP2 knockdown enhances the rate of EGFR degradation when cells are stimulated with low levels of EGF (1.5 ng/ml), which promotes EGFR recycling (Sigismund et al., 2008). Under these conditions, total EGFR levels remained nearly constant, dropping only to 95% of the starting levels during the 1-h stimulation (Fig. 3I). Notably, we did not observe any differences in EGFR levels between control and NECAP2 KD cells (Fig. 3I). Taken together, these data show that EGFR accumulates in early endosomes following NECAP2 depletion as a result of impaired EGFR recycling. In contrast, NECAP2 is not required for endosomal cargo sorting into multivesicular bodies for receptor degradation.

NECAP2 knockdown shifts TfnR into early endosomes

We next tested whether NECAP2 depletion also affects the recycling of the transferrin receptor (TfnR) and its ligand transferrin. TfnR is internalized through clathrin-mediated endocytosis and recycles from early endosomes through the fast Rab4a-dependent and the slow Rab4b- and Rab11a-dependent pathway. NECAP2 knockdown did not lead to changes in the cell surface levels of TfnR (Fig. 4A). However, NECAP2 depletion resulted in increased total levels of TfnR (Fig. 2C,D), suggesting that NECAP2 KD cells maintain normal receptor surface levels by upregulating TfnR expression. To test for changes in TfnR distribution, we quantified the percentage of TfnR that colocalized with markers for early endosomes (EEA1), recycling endosomes (Rab11a) and the trans-Golgi network (TGN46; also known as TGOLN2) in control and NECAP2 KD cells. We did not observe any changes in the amount of TfnR present in recycling endosomes or the trans-Golgi (Fig. 4B,C). In contrast, following NECAP2 depletion, a significantly larger pool of TfnR accumulated in early endosomes (Fig. 4B,C), suggesting that NECAP2 depletion also impairs TfnR recycling.

NECAP2 knockdown has no effect on slow transferrin recycling

To directly test for changes in TfnR recycling, we fed control and NECAP2 KD cells with fluorescently-labeled transferrin for 70 min, stripped off the surface pool and followed the loss of transferrin–Cy3 over time. Samples were taken every 15 min to test for changes in the slow recycling pathway. Notably, NECAP2 KD cells gained significantly higher amounts of transferrin–Cy3 during the labeling pulse (detected at the 0-min time point of the chase, Fig. 4D), consistent with the higher levels of TfnR expression in NECAP2 KD cells (Fig. 2C,D). During recycling, NECAP2 KD

Journal of Cell Science (2016) 129, 2625-2637 doi:10.1242/jcs.173708

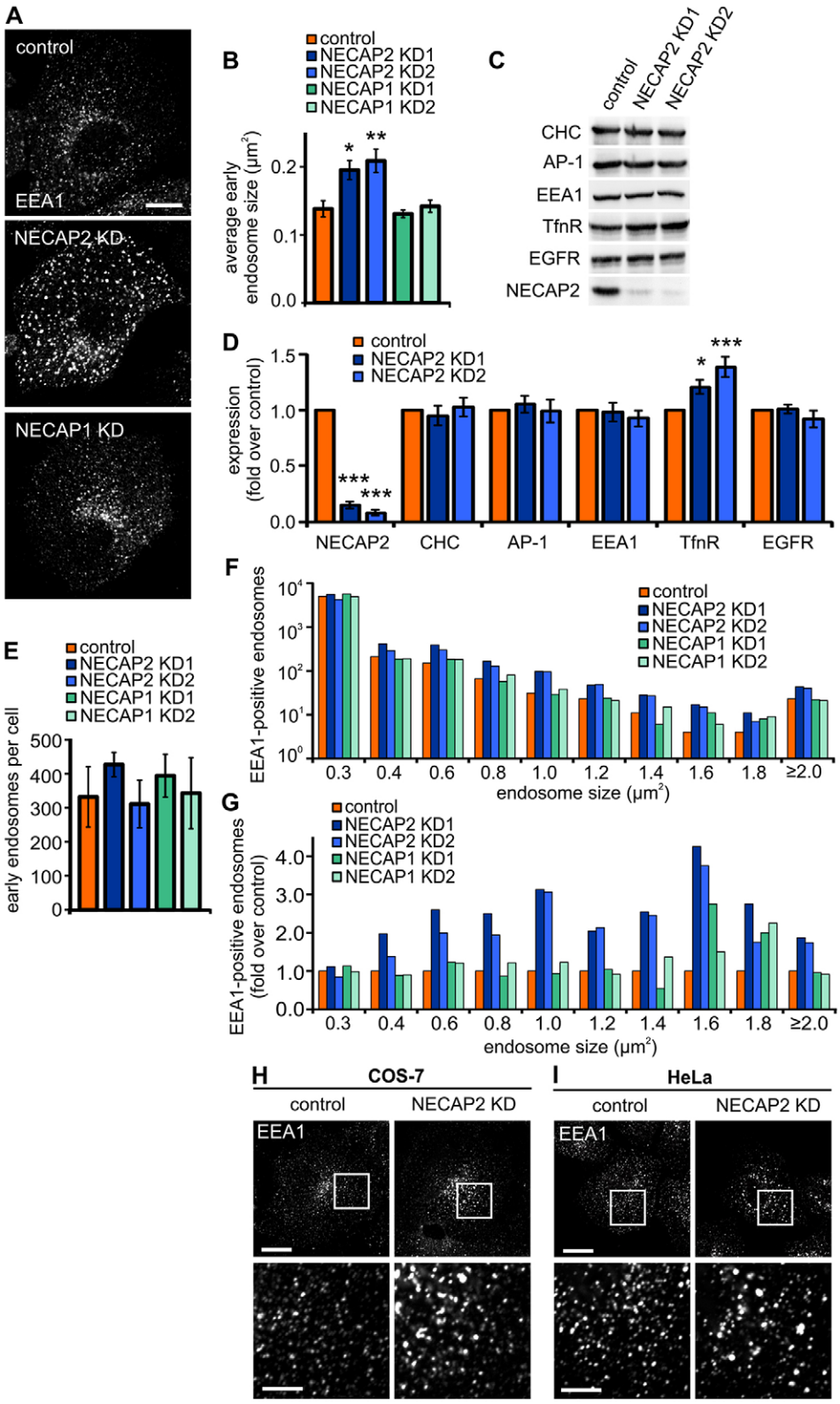

Fig. 2. Early-endosome enlargement in NECAP2 KD cells. (A) Confocal images of the immunofluorescence analysis of endogenous EEA1 expression in MCF10A control, NECAP2 KD and NECAP1 KD cells as indicated. Scale bar: 10 µm. (B,E) Quantification of the average size of early endosomes (B) and early endosome number per cell (E). (B,E–G) Mean±s.e.m., *N*=3 experiments, *n*=16–18 cells total per group, 5178–6772 endosomes total per group. (C) Western blot analysis of total protein lysates of control and NECAP2 KD cells for expression of various proteins as indicated. The γ-adaptin subunit was used to detect AP-1. CHC, clathrin heavy chain. (D) Quantification of data shown in C; mean±s.e.m., *N*=3 experiments. (B,D,E) Statistical analysis using one-way ANOVA followed by Dunnett's post-test revealed significant differences between control and knockdown cells for B,D, and no significant differences for E. **P*<0.05, ***P*<0.01, ****P*<0.001. (F) Quantification of endosome size distribution for the total number of endosomes analyzed in B,E, with the *y*-axis given on a log scale. (G) The same data as that in F, plotted as the fold change over control for each bin. (H,I) Confocal images of the immunofluorescence analysis of endogenous EEA1 expression in control and NECAP2 KD COS-7 (H) and HeLa cells (I). Boxes indicated in the top row show regions of interest magnified in the bottom row. Scale bars: 15 µm (low magnification images, top row); 5 µm (high magnification images, bottom row).

cells maintained higher levels of transferrin–Cy3 over time compared to control cells (Fig. 4D). However, replotting the curves by normalizing for starting levels of transferrin revealed that control and NECAP2 KD cells recycled transferrin–Cy3 with a similar rate and kinetics (Fig. 4E), indicating that NECAP2 has no effect on the slow recycling of transferrin–TfnR.

NECAP2 controls transferrin recycling along the fast recycling pathway

The fast recycling pathway sends receptors back to the cell surface within minutes (Hao and Maxfield, 2000; Sheff et al., 1999, 2002). As such, the rate of short-term internalization of transferrin–Cy3 transitions from a purely endocytic phase to a

Journal of Cell Science

Journal of Cell Science (2016) 129, 2625-2637 doi:10.1242/jcs.173708

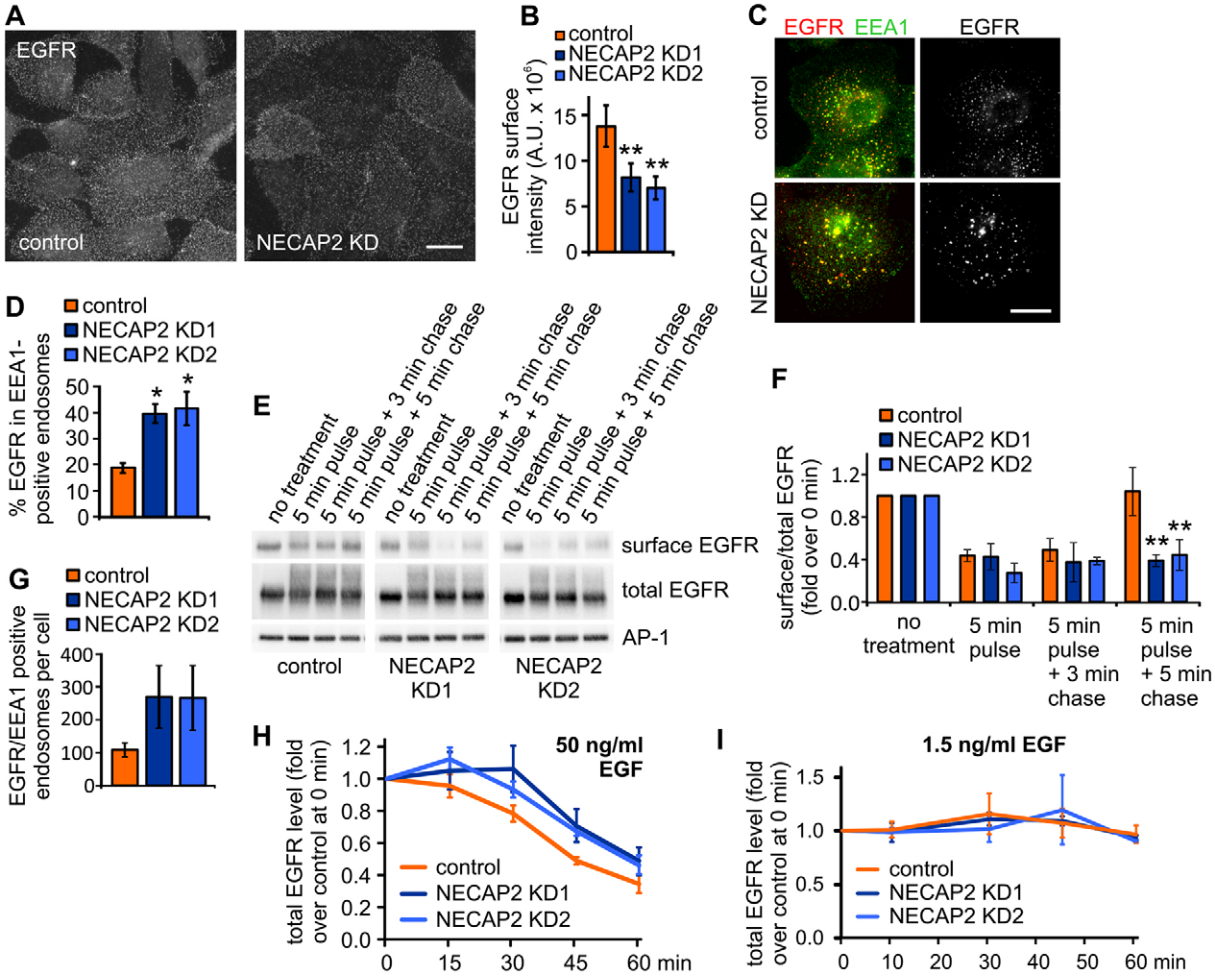

Fig. 3. NECAP2 controls EGFR recycling but not degradation. (A) Immunofluorescence analysis of the cell surface pool of endogenous EGFR in control and NECAP2 KD cells, as indicated. Scale bar: 20 µm. (B) Quantification of the fluorescence intensity images shown in A; mean±s.e.m., *N*=3 experiments, *n*=123–136 cells total per group. A.U., arbitrary units. Statistical analysis using repeated-measures one-way ANOVA followed by Bonferroni post-test revealed significant differences between control and NECAP2 KD cells, $^{**}P<0.01$. (C) Immunofluorescence analysis of endogenous EGFR and EEA1 in control and NECAP2 KD cells, as indicated. Scale bar: 20 µm. (D) Quantification of the fraction of total EGFR signal intensity that colocalized with EEA1; mean±s.e.m., *N*=3 experiments, *n*=77–92 cells per group. Statistical analysis using one-way ANOVA followed by Bonferroni post-test revealed significant differences between control and NECAP2 KD cells, $^{*}P<0.05$. (E) Western blot analysis of surface EGFR, total EGFR and AP-1 (γ-adaptin subunit) levels in control and NECAP2 KD HeLa cells with or without TGFα treatment (denoted by 'pulse'), as indicated. EGFR surface pools were antibody-labeled on ice prior to cell lysis and immunoprecipitation. (F) Quantification of EGFR surface levels from images shown in E; mean±s.e.m., *N*=3 experiments. Statistical analysis using two-way ANOVA followed by Bonferroni post-test revealed significant differences between control and NECAP2 KD cells for the 5 min chase; $^{**}P<0.01$. (G) Quantification of the number of EGFR- and EEA1-positive puncta in control and NECAP2 KD cells following stimulation with 1.5 ng/ml EGF; mean±s.e.m., *N*=3, *n*=47–50 cells per group. Statistical analysis using one-way ANOVA followed by Dunnett's post-test revealed no significant differences. (H,I) Quantification of EGFR degradation in control and NECAP2 KD cells over time following stimulation with 50 ng/ml (H) or 1.5 ng/ml EGF (I); mean±s.e.m., *N*=3. Statistical analysis using two-way ANOVA followed by Bonferroni post-test revealed no significant differences.

balance between endocytosis and fast recycling. NECAP2 depletion led to enhanced accumulation of transferrin–Cy3 within 5 min of continuous labeling at 37°C (Fig. 5A,B). Given that control and NECAP2 KD cells display similar levels of TfnR on the cell surface (Fig. 4A), and show no difference in the number of endocytic clathrin-coated pits and vesicles (Fig. 1B–D), transferrin and EGF internalization (Fig. 1E–M), and slow recycling (Fig. 4D,E), the intracellular accumulation of transferrin after 5 min of uptake is thus likely to be the result of impaired fast recycling.

To increase the temporal resolution of the assay, we analyzed the amount of intracellular transferrin–Cy3 every minute over a 5-min period in MCF10A cells. During the first two minutes, we detected no difference in the amounts of internalized transferrin–Cy3 between control and NECAP2 KD cells (Fig. 5C,D). These time points are likely to reflect the purely endocytic phase (Doyon et al., 2011; Saffarian et al., 2009). At 3 min, transferrin begins to reach early endosomes and, at this point, NECAP2 KD cells showed a trend towards accumulating higher amounts of transferrin–Cy3, resulting in a significant build-up at later time points (Fig. 5C,D). These results are consistent with the increase in internalized transferrin in COS-7 cells that was detected at only the longer 4-min time point but not at the solely endocytic 1-min time point upon quantitative measurement of infrared fluorescence (Fig. 1I,J). Taken together, these data further support a role for NECAP2 in the fast recycling pathway.

We next sought to directly test for changes in fast recycling. For this, we labeled control and NECAP2 KD MCF10A cells with

Journal of Cell Science (2016) 129, 2625-2637 doi:10.1242/jcs.173708

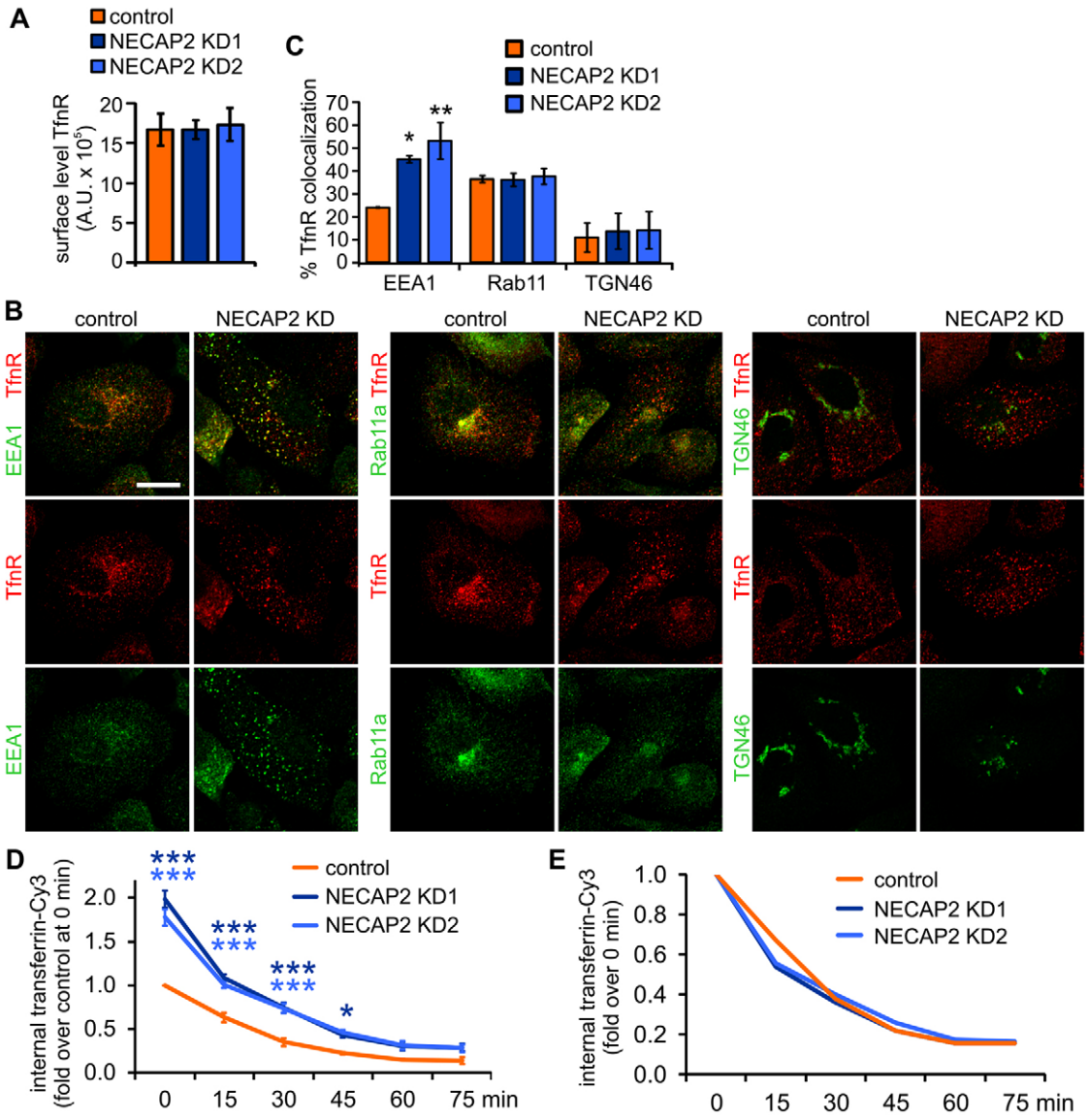

Fig. 4. NECAP2 does not control slow transferrin recycling. (A) Quantification of fluorescence intensity of the cell surface labeling of endogenous TfnR in control and NECAP2 KD cells; mean±s.e.m., *N*=3 experiments, *n*=85–101 cells per group. A.U., arbitrary units. (B) Confocal images of the immunofluorescence analysis of the degree of colocalization of endogenous TfnR with endogenous EEA1, Rab11a or TGN46 in control and NECAP2 KD cells, as indicated. Scale bar: 15 µm. (C) Quantification of the fraction of the total TfnR fluorescence signal colocalizing with the indicated markers; mean±s.e.m., *N*=3 experiments, *n*=12 cells total per group and marker. In A,C, statistical analysis using one-way ANOVA followed by Dunnett's post-tests revealed significant differences between control and NECAP2 KD cells for C, **P*<0.05, ***P*<0.01, and no significant differences were found for A. (D) Quantification of transferrin recycling in control and NECAP2 KD cells over time, as measured using the transferrin–Cy3 signal intensity; mean±s.e.m., *N*=4 experiments, *n*=66–137 cells per group and time point. Statistical analysis using two-way ANOVA followed by Bonferroni post-test revealed significant differences between control and NECAP2 KD cells; **P*<0.05, ****P*<0.001. (E) Same data as that shown in D, plotted by adjusting the 0-min time point to a value of 1 for each condition.

transferrin–Cy3 for 5 min at 37°C, which is enough time for transferrin to reach early endosomes, stripped off any surface label by acid-washing on ice, and chased cells with pre-warmed regular medium. Each minute, aliquots of cells were acid-washed on ice, fixed and the amount of transferrin–Cy3 remaining in the cells was quantified with fluorescence microscopy. These assays revealed that NECAP2 knockdown caused a significant delay in transferrin recycling within the first few minutes of the chase (Fig. 5E,F), directly demonstrating that NECAP2 controls fast recycling. Moreover, NECAP2 knockdown also impaired fast transferrin recycling in HeLa and COS-7 cells (Fig. 5G–J), confirming that NECAP2 is a general regulator of the fast recycling pathway.

NECAP2 is essential for recruitment of AP-1 to early endosomes

AP-1 and clathrin mediate receptor transport from early endosomes and the Golgi. On early endosomes, AP-1 is involved in both the fast and slow recycling pathway, and is recruited downstream of Rab4a and Rab4b, respectively (D'Souza et al., 2014; Perrin et al., 2013). Because NECAP1 depletion affects AP-2-positive forming vesicles at the cell surface and because NECAP2 binds to AP-1 (Ritter et al., 2004, 2013), we used immunofluorescence studies for the γ-adaptin subunit of AP-1 to test whether NECAP2 depletion affects the recruitment of AP-1 to early endosomes. Control MCF10A cells showed a prominent Golgi-associated pool of AP-1 and discrete AP-1-positive puncta in the periphery of the cell that

Journal of Cell Science (2016) 129, 2625-2637 doi:10.1242/jcs.173708

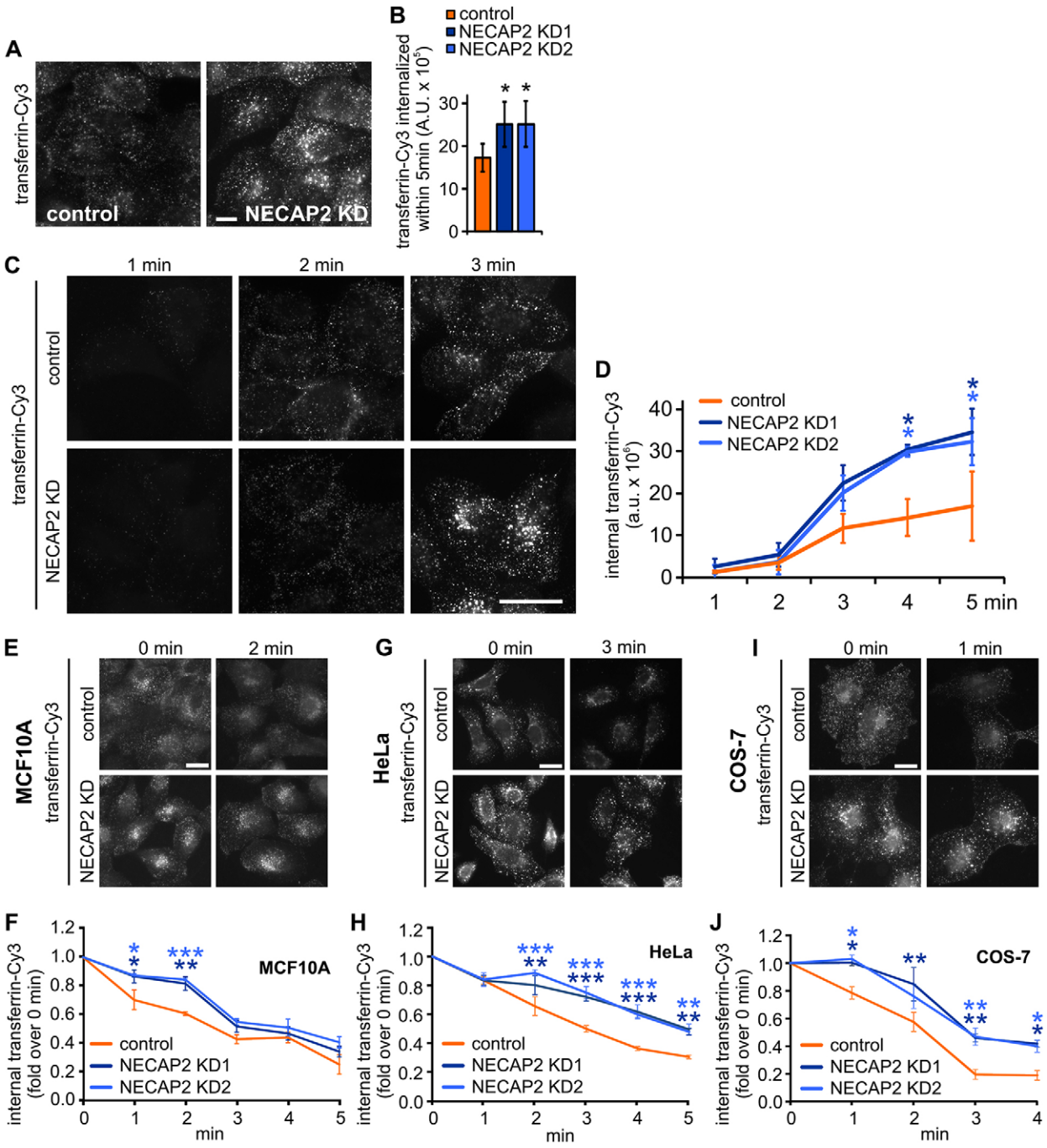

Fig. 5. NECAP2 controls transferrin recycling through the fast recycling pathway. (A) Fluorescence analysis of transferrin–Cy3 internalization within 5 min into control and NECAP2 KD cells as indicated. Scale bar: 10 µm. (B) Quantification of the fluorescence intensity shown in A; mean±s.e.m., *N*=4 experiments, *n*=142–156 cells total per group. (C) Fluorescence analysis of transferrin–Cy3 internalized over time by control and NECAP2 KD cells, as indicated. Scale bar: 10 µm. (D) Quantification of the signal intensity shown in C and of additional time points; mean±s.e.m., *N*=3 experiments, *n*=60–160 cells total per group and time point. (E,G,I) Immunofluorescence analysis of transferrin–Cy3 recycling over time in control and NECAP2 KD MCF10A (E), HeLa (G) and COS-7 cells (I). Scale bars: 20 µm. (F,H,J) Quantification of data shown in E,G,I; mean±s.e.m., *N*=3 experiments, *n*=8–29 cells per condition per time point for F, *n*=10–23 cells per condition per time point for H and *n*=4–14 cells per condition per time point for J. For D,F,H,J, statistical analysis using two-way ANOVA followed by Bonferroni post-test revealed significant differences between control and NECAP2 KD cells; **P*<0.05, ***P*<0.01, ****P*<0.001.

were also positive for EEA1 (Fig. 6A). NECAP2 KD cells maintained the Golgi pool of AP-1 (Fig. 6A) and showed no differences in the total expression levels of AP-1 and clathrin compared to control cells (Fig. 2C,D; Fig. 6B). However, NECAP2 depletion led to a selective loss of AP-1 from early endosomes (Fig. 6A,C). Consistently, we also observed a selective loss of AP-1 from early endosomes in HeLa and COS-7 cells (Fig. 6D,E). Thus, NECAP2 is required for the efficient recruitment of the AP-1–clathrin machinery to early endosomes in order to facilitate receptor recycling.

Journal of Cell Science (2016) 129, 2625-2637 doi:10.1242/jcs.173708

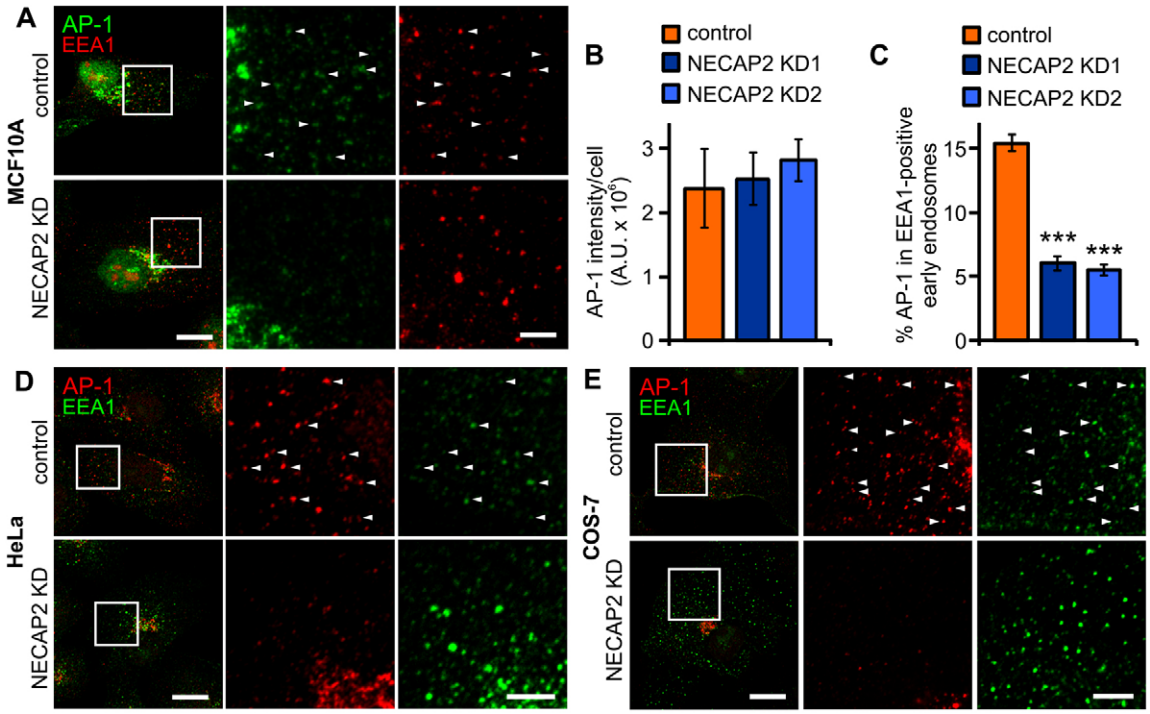

Fig. 6. NECAP2 is essential for AP-1 recruitment to early endosomes. (A,D,E) Immunofluorescence analysis of endogenous γ-adaptin subunit of AP-1 and EEA1 in control and NECAP2 KD MCF10A (A), HeLa (D) and COS-7 cells (E). Arrowheads indicate structures labeled by both proteins. Scale bars: 15 µm (low magnification images, left-hand column); 5 µm (high magnification images, middle and right-hand columns). Boxes indicated in the left-hand column show regions of interest magnified in the middle and right-hand columns. (B) Quantification of the total intensity levels of endogenous AP-1 by using immunofluorescence analysis in control and NECAP2 KD MCF10A cells; mean±s.e.m., *N*=3 experiments, *n*=15 cells total per group. A.U., arbitrary units. (C) Quantification of the fraction of the endogenous AP-1 signal intensity that colocalized with endogenous EEA1-positive early endosomes in control and NECAP2 KD MCF10A cells; mean±s.e.m., *N*=3. (B,C) Statistical analysis using one-way ANOVA followed by Dunnett's post-test revealed significant differences between control and NECAP2 KD cells for C, and no significant differences were found for B; ***$P<0.001$.

Multiple binding interfaces in NECAP2 are required for AP-1 recruitment to early endosomes

To determine how NECAP2 controls AP-1 recruitment to early endosomes and fast recycling, we performed rescue experiments with NECAP2 wild-type and point mutants. Re-expression of wild-type NECAP2 rescued the peripheral punctate pool of AP-1, although AP-1 levels were not fully restored (Fig. 7A,B). We have noticed that overexpression of NECAP2 results in a mislocalization of several NECAP2-binding partners, including AP-1 (data not shown); thus, although we tightly controlled the expression levels of our rescue constructs by using lentiviral delivery and excluded cells with high expression levels from the analysis, a fraction of the cells are likely to have expressed either too little or too much NECAP2 to achieve complete rescue.

Notably, NECAP2 variants in which the C-terminal AP-1-binding motif or the N-terminal PH domain had been inactivated failed to rescue the knockdown phenotype (Fig. 7A,B). We used co-immunoprecipitation to confirm that all rescue constructs, with the exception of the AP-1 motif mutant, interacted with AP-1 to similar extents (Fig. 7C), excluding side-effects of the point mutations on NECAP2 folding and stability. Taken together, these data demonstrate that the ability of NECAP2 to interact with the ear domain of the γ-adaptin subunit of AP-1 and with PH-domain-binding partners is essential for NECAP2 function. This further suggests a central role for NECAP2 in the formation of a protein network that promotes recycling vesicle formation on early endosomes and fast receptor recycling (Fig. 7D). Finally, expression of wild-type NECAP1 does not rescue the NECAP2 knockdown phenotype (Fig. 7A,B), providing further proof that the two mammalian NECAP-family members are functionally divergent.

DISCUSSION

The NECAP proteins show a high degree of sequence similarity and share a common structural organization, including two peptide motifs for interaction with the clathrin adapter proteins AP-1 and AP-2 (Ritter et al., 2007, 2004, 2003). We have recently shown that NECAP1 cooperates with AP-2 to ensure efficient vesicle formation for clathrin-mediated endocytosis (Ritter et al., 2013); in contrast, the data presented here demonstrate a central role for NECAP2 in AP-1-mediated fast recycling from early endosomes. Furthermore, each NECAP protein failed to rescue the knockdown phenotype of the other family member (Fig. 7A,B; Ritter et al., 2013). Taken together, these data demonstrate that NECAP1 and NECAP2 have functionally diverged to selectively regulate clathrin-mediated sorting at distinct cellular locations. Future studies into the molecular determinants that link the NECAPs into their respective pathway might begin to unravel how related protein machineries adapt to fulfill similar yet distinct functions at different localizations within the cell.

Casanova and colleagues have recently deciphered a small GTPase cascade downstream of Rab4a for AP-1 recruitment to early endosomes (D'Souza et al., 2014). Active Rab4a leads to the recruitment and activation of Arl1 at early endosomes and the subsequent recruitment of the Arl1 effector proteins BIG1 and BIG2. The BIG proteins then function as GEFs for Arf1 and Arf3, which in turn recruit AP-1 (D'Souza et al., 2014). Because NECAP2 depletion leads to a loss of AP-1 from early endosomes, it will be interesting to determine whether NECAP2 is required for full

Journal of Cell Science (2016) 129, 2625-2637 doi:10.1242/jcs.173708

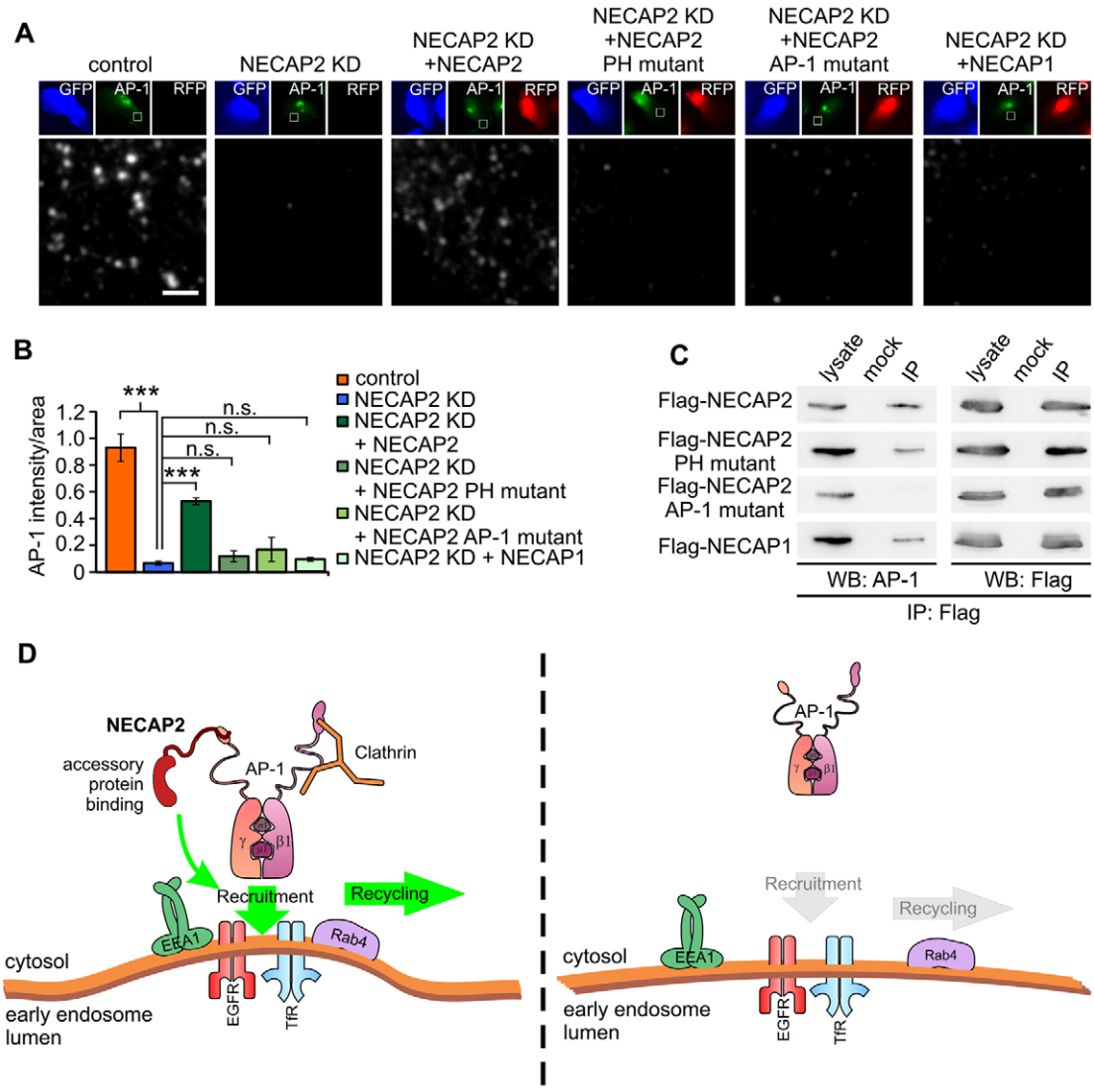

Fig. 7. The PH domain and AP-1-binding motif of NECAP2 are crucial for AP-1 recruitment to early endosomes. (A) Immunofluorescence analysis of endogenous AP-1 (γ-adaptin subunit). The top three panels of each image (left to right) show the soluble GFP marker for transduction with control and NECAP2 KD viruses in blue, endogenous AP-1 in green and the RFP signal of rescue constructs in red, as indicated. The bottom panel of each image shows the magnified area outlined in white in the AP-1 panel. Scale bar: 2 µm. (B) Quantification of the total levels of endogenous AP-1 intensity by immunofluorescence analysis in control, NECAP2 KD and NECAP2 KD+rescue cells; mean±s.e.m., *N*=3 experiments, *n*=30 cells per group. Results displayed as the intensity of AP-1 per area of the cell (µm^2). Analysis was performed by subtracting the Golgi pool of AP-1 from the analysis to account for only endosomal puncta. Co-staining for an early endosome marker could not be performed owing to lack of additional channels for image acquisition. Statistical analysis using one-way ANOVA followed by Dunnett's post-test revealed significant differences between NECAP2 KD and control and NECAP2 wild-type rescue cells, and no significant differences were found between NECAP2 KD cells and cells rescued with the NECAP2 PH mutant, NECAP2 AP-1 mutant, or NECAP1; ***P<0.001. n.s., not significant. (C) Western blot (WB) analysis of co-immunoprecipitation of AP-1 with various Flag-tagged NECAP variants, as indicated. Lysate equals 10% of the total protein lysate used for the immunoprecipitation (IP). (D) Model of NECAP2 function. The left panel depicts AP-1 recruitment to early endosomes in the presence of NECAP2. NECAP2 interacts with the AP-1 γ-ear through the C-terminal AP-1 binding motif, whereas the NECAP2 PH domain promotes interactions with accessory proteins for recycling vesicle formation. In the absence of NECAP2 (right panel), AP-1 has less affinity for early endosomes, leading to impaired recruitment and fast recycling.

activation of this GTPase cascade. Alternatively, NECAP2 could be part of a second mechanism that contributes to and is required for AP-1 recruitment to early endosomes. Our rescue studies revealed that NECAP2 function depends on the C-terminal AP-1-binding motif and the protein-binding interface of the N-terminal PH domain. In NECAP1, the PH domain allows for efficient recruitment of endocytic accessory proteins to the forming vesicle, and loss of PH domain function is sufficient to impair vesicle formation (Ritter et al., 2013). It is thus tempting to speculate that the PH domain of NECAP2 fulfils a similar role during recycling vesicle formation at early endosomes. Here, the effect of loss of NECAP2 or PH-domain-mediated interactions is more severe, leading to the loss of AP-1 from the organelle. This might reflect that a less-complex protein machinery is involved at early endosomes compared to the endocytic clathrin machinery at the plasma membrane. In this scenario, depletion of a single component, such as NECAP2, would lower the chance of successful initiation and/or stabilization of the protein network and imbalance the formation of the clathrin coat.

Interestingly, the Rab4a GTPase cascade also promotes the recruitment of additional clathrin adapters, AP-3 and GGA3

Journal of Cell Science (2016) 129, 2625-2637 doi:10.1242/jcs.173708

(D'Souza et al., 2014). It remains currently unknown if this reflects the cooperation and/or interdependency of different clathrin adapters during recycling vesicle formation similar to the AP-1-dependent association of GGA2 with clathrin-coated vesicles, and the cooperation of AP-1 and GGAs in mannose-6-phosphate receptor sorting in mammalian cells, and the GGA2-supported recruitment of AP-1 to the trans-Golgi network in yeast (Daboussi et al., 2012; Doray et al., 2002; Hirst et al., 2012). Alternatively, the involvement of multiple adapters could increase the variety of cargo utilizing the Rab4a pathway. For example, in polarized epithelial cells, the two AP-1 complex variants, AP-1A and AP-1B, bind to cargo with different affinities, thereby promoting differential sorting (Guo et al., 2013). Interestingly, *in vitro* binding studies suggest that NECAP2 also interacts with GGA1 and GGA2 (Mattera et al., 2004), while it currently remains unknown if NECAP2 also interacts with GGA3. We have not detected any changes in GGA3 localization due to NECAP2 depletion, although this aspect will require further investigation with improved reagents for GGA3.

Cargo sorting into the endocytic recycling pathways has been considered a signal-independent default route for receptors. The high surface-to-volume ratio of newly formed vesicles and tubules is thought to allow for geometry-based sorting of membrane-bound molecules away from soluble material or receptors actively retained in the early endosomal lumen (Dunn et al., 1989; Linderman and Lauffenburger, 1988; Mayor et al., 1993; Verges et al., 1999). To date, a more detailed understanding of the contributions of Rabs, Arfs and sorting nexins to receptor sorting suggests that recycling pathways and/or machineries can create cargo selectivity. For example, Rab25 differentially recycles integrin dependent on the activation state of the receptor (Dozynkiewicz et al., 2012). On early endosomes, Rab35 and Arf6 counter-regulate each other to balance Rab35-dependent cadherin and Arf6-dependent integrin recycling (Allaire et al., 2013). In addition, Rab4a and Arf6 cooperate in the recycling of Met receptor (Parachoniak et al., 2011). It will be interesting to see if NECAP2 functions in all Rab4a-mediated recycling events or with a specific subset of clathrin adaptors and/or cargo.

MATERIALS AND METHODS

Antibodies and reagents

Antibodies directed against AP-1 (clone 88; WB: 1:1000; IF: 1:100), CHC (CHC17, clone 23; 1:1000) and EEA1 (mouse, clone 14; WB: 1:10,000; IF: 1:500) were purchased from BD Transduction Laboratories. Antibodies against EGFR (sc-120 for recycling and immunofluorescence studies, 1:100; sc-03 for western blot; 1:500) and TfnR (sc-65882; WB: 1:500; IF: 1:200) were obtained from Santa Cruz Biotechnology. The antibody against EEA1 (rabbit, 2411S; 1:50) was from Cell Signaling Technology, the anti-TGN46 antibody (ab50595; 1:500) was from Abcam, the anti-Rab11 antibody (71-5300; 1:100) was from Thermo Scientific and the NECAP2 (HPA028077; 1:250) and Flag (M2; WB: 1:20,000; IF: 1:50,000) antibodies were from Sigma-Aldrich. The antibody raised against NECAP1 has been described previously (1:5000) (Ritter et al., 2003). Human transferrin–Cy3 was purchased from Jackson ImmunoResearch, human transferrin-Alexa-Fluor-647 and EGF-Alexa-Fluor-647 were purchased from Thermo Scientific and recombinant human TGFα (100-16A; see below under 'EGFR recycling') was purchased from PeproTech.

Quantification and statistics

Western blots and fluorescence images were quantified using ImageJ (Schneider et al., 2012). For fluorescence analysis of cells, signal intensities were measured as integrated densities and the size was measured using signal area. Colocalization of two markers was quantified using the colocalization plugin for ImageJ. The plugin allows determination of the fraction of signal area of one marker that overlaps and/or colocalizes with the area occupied by a second marker. The resulting mask is then redirected to the individual channels of the original image to determine the signal intensity within the colocalized area. After determining the total signal intensity of the marker, one can calculate the colocalized fraction of signal intensity. Cell numbers were tracked manually. GraphPad Prism 5 was used to perform statistical analyses; details about data analysis and post-tests are included in the figure legends where appropriate.

Total protein lysates

Cells were lysed with ice-cold lysis buffer (10 mM Hepes, pH 7.4, 150 mM NaCl, 2 mM EGTA, 2 mM EDTA, 25 mM sodium pyrophosphate, 50 mM β-glycerophosphate, 1% Triton X-100, 50 mM sodium fluoride, 1 mM sodium orthovanadate, 0.83 mM benzamidine, 0.23 mM PMSF, 0.5 µg/ml aprotinin, 0.5 µg/ml leupeptin) and centrifuged for 2 min at 21,000 ***g*** to remove cell fragments. Equal amounts of total protein were resolved by SDS-PAGE, and expression levels were determined by western blotting.

Cell culture

MFC10A, HeLa, HEK 293-T and COS-7 cells were obtained from American Type Culture Collection. MCF10A cells were cultured as described previously by Debnath et al. (2003), with the omission of penicillin-streptomycin in all solutions. HeLa, COS-7 and HEK 293-T cells were cultured in Dulbecco's modified Eagle's medium (DMEM) high glucose (SH30243, Hyclone Laboratories) supplemented with 10% iron-supplemented calf serum (Hyclone) under a 5%-CO_2-containing water-saturated atmosphere. For transient protein expression, HEK 293-T cells were transfected using calcium phosphate, and COS-7 and HeLa cells were transfected using jetPrime (Polyplus Transfection, New York, NY) according to the manufacturer's recommendations. Five hours after addition of the transfection mix to the cells, the medium was removed and replaced with regular culture medium. For cell imaging, cells were plated on 12-mm poly-L-lysine (PLL)-coated coverslips, no 1.5 (NeuVitro Corporation, Vancouver, WA).

Protein knockdown

Control and NECAP2 knockdown viruses were generated and produced as previously described (Ritter et al., 2013). The two NECAP2 target sequences start at nucleotides 341 (KD1) and 388 (KD2) of the human *NECAP2* open reading frame (accession number NM_018090). The NECAP1 KD constructs target two independent nucleotide sequences within the human *NECAP1* transcript and have been described previously (Ritter et al., 2013). For NECAP knockdown, cells were plated late in the day before transduction. Within 16 h after plating, the culture medium was replaced with regular culture medium supplemented with 6 µg/ml polybrene (Sigma-Aldrich), and viruses were added at a multiplicity of infection (MOI) of 5. After 5 h, medium was replaced with fresh culture medium, and the cells were cultivated until assays were performed 5 or 6 days after transduction.

Immunofluorescence

For intracellular localization studies, cells were washed with PBS, fixed with 2% paraformaldehyde in PBS for 10 min at room temperature and permeabilized with 0.2% Triton X-100 in PBS for all antibodies but Rab11a. Antibodies were diluted with 0.02% Triton X-100 and incubated at room temperature. For detection of Rab11a, cells were fixed with 2% paraformaldehyde in PBS for 10 min at room temperature and incubated with primary and secondary antibodies diluted in PBS+0.05% saponin. For cell surface staining, cells were processed as described above but omitting the cell permeabilization step and diluting antibodies in PBS alone. Secondary antibodies were labeled with Alexa-Fluor-555 or Alexa-Fluor-647, and samples were mounted using Prolong Diamond antifade reagent (Thermo Scientific).

Fluorescence imaging

Images were collected on a Zeiss Observer D1 equipped with Colibri.2 and HXP light sources and an ORCA-Flash 4.0 digital CMOS camera (Hamamatsu, Bridgewater, NJ). For some experiments, as indicated in the figure legend, images were collected on a Zeiss LSM 700 confocal

Journal of Cell Science (2016) 129, 2625-2637 doi:10.1242/jcs.173708

microscope. For all quantitative analyses, image acquisition settings were set based on the longest time points or brightest conditions such that signals were not saturated according to the range indicator feature in the ZEN imaging software (ZEISS, Germany), and settings were kept constant for all images.

EGFR internalization

Cells were plated in replicates two days before the experiment, starved overnight in serum-free medium and incubated with 2 ng/ml EGF–Alexa-Fluor-647 in cold serum-free medium on ice for 1 h. One set (surface) was washed with PBS, fixed with ice-cold 2% paraformaldehyde in PBS for 20 min on ice, washed again and mounted. The second set was incubated with pre-warmed serum-free medium for 2.5 min at 37°C, acid-washed on ice to remove residual EGF from the cell surface, and then processed as described above.

EGFR recycling

For EGFR recycling following TGFα treatment, cells were plated 1 to 2 days before the experiment and starved in serum-free medium for 1 h. The first set of cells was immediately placed on ice and processed as described below. The other three sets of cells were incubated with pre-warmed serum-free medium containing 10 nM TGFα for 4 min at 37°C to allow for EGFR internalization, then acid-washed on ice. Two sets of cells were returned to 37°C in pre-warmed serum-free medium for 3 and 5 min to allow for receptor recycling, then acid-washed on ice. All samples were incubated for 45 min with an antibody directed against the extracellular region of EGFR that had been diluted 1:100 in regular culture medium to label the surface pool of EGFR. Cells were washed and lysed in RIPA buffer supplemented with 0.83 mM benzamidine, 0.23 mM PMSF, 0.5 µg/ml aprotinin, 0.5 µg/ml leupeptin. Lysates were cleared by centrifugation at 200,000 ***g*** for 20 min at 4°C, and aliquots of 100 µg of total protein were incubated with 10 µl of sheep anti-mouse IgG Dynabeads (11201D, Thermo Scientific) for 1 h on an orbital shaker at 4°C. Bound proteins were resolved by SDS-PAGE, and EGFR levels were detected by western blotting.

EGFR degradation

Cells were plated in replicates for each time point 1 to 2 days before the assay. On the day of the experiment, cells were stimulated with 1.5 or 50 ng/ml EGF in pre-warmed regular culture medium for varying lengths of time at 37°C, shifted onto ice, washed with ice-cold PBS and lysed with ice-cold lysis buffer. Cells were scraped and disrupted by mechanical force. Supernatants were resolved by SDS-PAGE, and total EGFR levels were detected by western blotting.

Transferrin internalization

For analysis by fluorescence imaging, cells were plated in replicates for each time point 1 to 2 days before the assay. On the day of the experiment, cells were fed with human-transferrin–Cy3 (13 µg/ml) in pre-warmed regular culture medium for varying lengths of time at 37°C. For each time point, cells were shifted onto ice, and the surface pool of transferrin–Cy3 was stripped off by acid washing. Cells were then washed with ice-cold PBS, fixed with ice-cold 2% paraformaldehyde in PBS for 20 min on ice, washed again and mounted. For quantitative analysis of infrared fluorescence, four sets of cells were incubated with pre-warmed serum-free medium for 2 h at 37°C. One set was immediately placed on ice, and washed and lysed as described below for the 'no treatment' samples. The other three sets of cells were incubated with transferrin–Alexa-Fluor-647 (13 µg/ml) in serum-free medium on ice for 30 min to label the surface pool of TfnR. Two cell sets were then incubated with pre-warmed serum-free medium at 37°C for 1 or 4 min to allow for internalization, followed by an acid wash on ice. All sets of cells were washed 2–3 times with cold PBS on ice, lysed in RIPA buffer supplemented with 0.83 mM benzamidine, 0.23 mM PMSF, 0.5 µg/ml aprotinin and 0.5 µg/ml leupeptin, and even amounts of total protein extract were separated by SDS-PAGE. The level of transferrin–Alexa-Fluor-647 in each extract was quantified by measuring the infrared fluorescence using an Odyssey imaging system (LI-COR Biosciences), and clathrin heavy chain (CHC) levels were detected by western blotting.

Transferrin recycling

For transferrin recycling assays, cells were fed with human transferrin–Cy3 (13 µg/ml) in regular medium for various lengths of time at 37°C. The cells were then placed on ice, and surface-bound transferrin was removed by acid washing, followed by a PBS wash. The 0-min time point was fixed with 2% paraformaldehyde in PBS for 20 min on ice, washed and mounted. The samples for later time points were shifted to 37°C and incubated with pre-warmed regular medium. For each time point, samples were placed on ice, washed with PBS and processed as described for the 0-min sample.

Rescue studies

Control and NECAP2 KD cells were plated in replicates 2 to 3 days before the assay and transduced the day before the assay with RFP–Flag-tagged wild-type NECAP2, or NECAP1, the NECAP2 PH mutant (containing an alanine substitution at residue arginine 101; R101A), or NECAP2 AP-1 mutant (containing a double alanine substitution at residues tryptophan 243 and phenylalanine 246; W243A F246A) at an MOI of 2 following the transduction protocol described for protein knockdown. The intracellular localization of endogenous AP-1 was determined by immunofluorescence using Alexa-Fluor-647 conjugated secondary antibodies.

Immunoprecipitation

HEK-293T cells were plated at 3.5×10^6 cells per 10-cm dish 1 day before transfection and then transfected with 5 µg of DNA per dish for the various NECAP expression constructs. The following day, cells were lysed in 10 mM HEPES, pH 7.4, 50 mM NaCl, 1% triton, 0.83 mM benzamidine, 0.23 mM PMSF, 0.5 µg/ml aprotinin and 0.5 µg/ml leupeptin. Lysates were cleared by centrifugation at 200,000 ***g*** for 20 min at 4°C, followed by pre-clearing with protein G agarose beads (Thermo Scientific). Flag-tagged NECAP proteins were isolated by immunoprecipitation using the Flag M2 antibody (Sigma-Aldrich), and bound proteins were resolved by SDS-PAGE and detected by western blotting.

Acknowledgements

We thank Dr Mikel Garcia-Marcos (Boston University) for helpful discussions and assistance with the quantitative infrared fluorescence measurements.

Competing interests

The authors declare no competing or financial interests.

Author contributions

J.P.C. and B.R. conceived, designed, executed and analyzed the data being published, and prepared the manuscript. L.T.A. and M.D.S. executed and analyzed experiments.

Funding

This research received no specific grant from any funding agency in the public, commercial or not-for-profit sectors.

References

Allaire, P. D., Seyed Sadr, M., Chaineau, M., Seyed Sadr, E., Konefal, S., Fotouhi, M., Maret, D., Ritter, B., Del Maestro, R. F. and McPherson, P. S. (2013). Interplay between Rab35 and Arf6 controls cargo recycling to coordinate cell adhesion and migration. *J. Cell Sci.* **126**, 722-731.

Antonescu, C. N., Aguet, F., Danuser, G. and Schmid, S. L. (2011). Phosphatidylinositol-(4,5)-bisphosphate regulates clathrin-coated pit initiation, stabilization, and size. *Mol. Biol. Cell* **22**, 2588-2600.

Bhuin, T. and Roy, J. K. (2015). Rab11 in disease progression. *Int. J. Mol. Cell. Med.* **4**, 1-8.

Bitsikas, V., Correa, I. R., Jr. and Nichols, B. J. (2014). Clathrin-independent pathways do not contribute significantly to endocytic flux. *Elife* **3**, e03970.

Blondeau, F., Ritter, B., Allaire, P. D., Wasiak, S., Girard, M., Hussain, N. K., Angers, A., Legendre-Guillemin, V., Roy, L., Boismenu, D. et al. (2004). Tandem MS analysis of brain clathrin-coated vesicles reveals their critical involvement in synaptic vesicle recycling. *Proc. Natl. Acad. Sci. USA* **101**, 3833-3838.

Daboussi, L., Costaguta, G. and Payne, G. S. (2012). Phosphoinositide-mediated clathrin adaptor progression at the trans-Golgi network. *Nat. Cell Biol.* **14**, 239-248.

Debnath, J., Muthuswamy, S. K. and Brugge, J. S. (2003). Morphogenesis and oncogenesis of MCF-10A mammary epithelial acini grown in three-dimensional basement membrane cultures. *Methods* **30**, 256-268.

Doray, B., Ghosh, P., Griffith, J., Geuze, H. J. and Kornfeld, S. (2002). Cooperation of GGAs and AP-1 in packaging MPRs at the trans-Golgi network. *Science* **297**, 1700-1703.
Doyon, J. B., Zeitler, B., Cheng, J., Cheng, A. T., Cherone, J. M., Santiago, Y., Lee, A. H., Vo, T. D., Doyon, Y., Miller, J. C. et al. (2011). Rapid and efficient clathrin-mediated endocytosis revealed in genome-edited mammalian cells. *Nat. Cell Biol.* **13**, 331-337.
Dozynkiewicz, M. A., Jamieson, N. B., MacPherson, I., Grindlay, J., van den Berghe, P. V. E., von Thun, A., Morton, J. P., Gourley, C., Timpson, P., Nixon, C. et al. (2012). Rab25 and CLIC3 collaborate to promote integrin recycling from late endosomes/lysosomes and drive cancer progression. *Dev. Cell* **22**, 131-145.
Dunn, K. W., McGraw, T. E. and Maxfield, F. R. (1989). Iterative fractionation of recycling receptors from lysosomally destined ligands in an early sorting endosome. *J. Cell Biol.* **109**, 3303-3314.
D'Souza, R. S., Semus, R., Billings, E. A., Meyer, C. B., Conger, K. and Casanova, J. E. (2014). Rab4 orchestrates a small GTPase cascade for recruitment of adaptor proteins to early endosomes. *Curr. Biol.* **24**, 1187-1198.
Ehrlich, M., Boll, W., van Oijen, A., Hariharan, R., Chandran, K., Nibert, M. L. and Kirchhausen, T. (2004). Endocytosis by random initiation and stabilization of clathrin-coated pits. *Cell* **118**, 591-605.
French, A. R., Sudlow, G. P., Wiley, H. S. and Lauffenburger, D. A. (1994). Postendocytic trafficking of epidermal growth factor-receptor complexes is mediated through saturable and specific endosomal interactions. *J. Biol. Chem.* **269**, 15749-15755.
Grant, B. D. and Donaldson, J. G. (2009). Pathways and mechanisms of endocytic recycling. *Nat. Rev. Mol. Cell Biol.* **10**, 597-608.
Guo, X., Mattera, R., Ren, X., Chen, Y., Retamal, C., González, A. and Bonifacino, J. S. (2013). The adaptor protein-1 mu1B subunit expands the repertoire of basolateral sorting signal recognition in epithelial cells. *Dev. Cell* **27**, 353-366.
Hao, M. and Maxfield, F. R. (2000). Characterization of rapid membrane internalization and recycling. *J. Biol. Chem.* **275**, 15279-15286.
Henriksen, L., Grandal, M. V., Knudsen, S. L. J., van Deurs, B. and Grøvdal, L. M. (2013). Internalization mechanisms of the epidermal growth factor receptor after activation with different ligands. *PLoS ONE* **8**, e58148.
Hirst, J., Borner, G. H. H., Antrobus, R., Peden, A. A., Hodson, N. A., Sahlender, D. A. and Robinson, M. S. (2012). Distinct and overlapping roles for AP-1 and GGAs revealed by the "knocksideways" system. *Curr. Biol.* **22**, 1711-1716.
Kelly, B. T. and Owen, D. J. (2011). Endocytic sorting of transmembrane protein cargo. *Curr. Opin. Cell Biol.* **23**, 404-412.
Kirchhausen, T., Owen, D. and Harrison, S. C. (2014). Molecular structure, function, and dynamics of clathrin-mediated membrane traffic. *Cold Spring Harb. Perspect. Biol.* **6**, a016725.
Kornilova, E., Sorkina, T., Beguinot, L. and Sorkin, A. (1996). Lysosomal targeting of epidermal growth factor receptors via a kinase-dependent pathway is mediated by the receptor carboxyl-terminal residues 1022–1123. *J. Biol. Chem.* **271**, 30340-30346.
Linderman, J. J. and Lauffenburger, D. A. (1988). Analysis of intracellular receptor/ligand sorting in endosomes. *J. Theor. Biol.* **132**, 203-245.
Maritzen, T., Schachtner, H. and Legler, D. F. (2015). On the move: endocytic trafficking in cell migration. *Cell. Mol. Life Sci.* **72**, 2119-2134.
Mattera, R., Ritter, B., Sidhu, S. S., McPherson, P. S. and Bonifacino, J. S. (2004). Definition of the consensus motif recognized by gamma-adaptin ear domains. *J. Biol. Chem.* **279**, 8018-8028.
Mayor, S., Presley, J. F. and Maxfield, F. R. (1993). Sorting of membrane components from endosomes and subsequent recycling to the cell surface occurs by a bulk flow process. *J. Cell Biol.* **121**, 1257-1269.
McMahon, H. T. and Boucrot, E. (2011). Molecular mechanism and physiological functions of clathrin-mediated endocytosis. *Nat. Rev. Mol. Cell Biol.* **12**, 517-533.
Mettlen, M., Loerke, D., Yarar, D., Danuser, G. and Schmid, S. L. (2010). Cargo- and adaptor-specific mechanisms regulate clathrin-mediated endocytosis. *J. Cell Biol.* **188**, 919-933.
Parachoniak, C. A., Luo, Y., Abella, J. V., Keen, J. H. and Park, M. (2011). GGA3 functions as a switch to promote Met receptor recycling, essential for sustained ERK and cell migration. *Dev. Cell* **20**, 751-763.
Perrin, L., Lacas-Gervais, S., Gilleron, J., Ceppo, F., Prodon, F., Benmerah, A., Tanti, J.-F. and Cormont, M. (2013). Rab4b controls an early endosome sorting event by interacting with the gamma-subunit of the clathrin adaptor complex 1. *J. Cell Sci.* **126**, 4950-4962.
Raiborg, C. and Stenmark, H. (2009). The ESCRT machinery in endosomal sorting of ubiquitylated membrane proteins. *Nature* **458**, 445-452.
Ritter, B., Philie, J., Girard, M., Tung, E. C., Blondeau, F. and McPherson, P. S. (2003). Identification of a family of endocytic proteins that define a new alpha-adaptin ear-binding motif. *EMBO Rep.* **4**, 1089-1095.
Ritter, B., Denisov, A. Y., Philie, J., Deprez, C., Tung, E. C., Gehring, K. and McPherson, P. S. (2004). Two WXXF-based motifs in NECAPs define the specificity of accessory protein binding to AP-1 and AP-2. *EMBO J.* **23**, 3701-3710.
Ritter, B., Denisov, A. Y., Philie, J., Allaire, P. D., Legendre-Guillemin, V., Zylbergold, P., Gehring, K. and McPherson, P. S. (2007). The NECAP PHear domain increases clathrin accessory protein binding potential. *EMBO J.* **26**, 4066-4077.
Ritter, B., Murphy, S., Dokainish, H., Girard, M., Gudheti, M. V., Kozlov, G., Halin, M., Philie, J., Jorgensen, E. M., Gehring, K. et al. (2013). NECAP 1 regulates AP-2 interactions to control vesicle size, number, and cargo during clathrin-mediated endocytosis. *PLoS Biol.* **11**, e1001670.
Roepstorff, K., Grandal, M. V., Henriksen, L., Knudsen, S. L. J., Lerdrup, M., Grøvdal, L., Willumsen, B. M. and van Deurs, B. (2009). Differential effects of EGFR ligands on endocytic sorting of the receptor. *Traffic* **10**, 1115-1127.
Saffarian, S., Cocucci, E. and Kirchhausen, T. (2009). Distinct dynamics of endocytic clathrin-coated pits and coated plaques. *PLoS Biol.* **7**, e1000191.
Schneider, C. A., Rasband, W. S. and Eliceiri, K. W. (2012). NIH Image to ImageJ: 25 years of image analysis. *Nat. Methods* **9**, 671-675.
Sheff, D. R., Daro, E. A., Hull, M. and Mellman, I. (1999). The receptor recycling pathway contains two distinct populations of early endosomes with different sorting functions. *J. Cell Biol.* **145**, 123-139.
Sheff, D., Pelletier, L., O'Connell, C. B., Warren, G. and Mellman, I. (2002). Transferrin receptor recycling in the absence of perinuclear recycling endosomes. *J. Cell Biol.* **156**, 797-804.
Sigismund, S., Argenzio, E., Tosoni, D., Cavallaro, E., Polo, S. and Di Fiore, P. P. (2008). Clathrin-mediated internalization is essential for sustained EGFR signaling but dispensable for degradation. *Dev. Cell* **15**, 209-219.
van der Sluijs, P., Hull, M., Webster, P., Mâle, P., Goud, B. and Mellman, I. (1992). The small GTP-binding protein rab4 controls an early sorting event on the endocytic pathway. *Cell* **70**, 729-740.
Verges, M., Havel, R. J. and Mostov, K. E. (1999). A tubular endosomal fraction from rat liver: biochemical evidence of receptor sorting by default. *Proc. Natl. Acad. Sci. USA* **96**, 10146-10151.
Welz, T., Wellbourne-Wood, J. and Kerkhoff, E. (2014). Orchestration of cell surface proteins by Rab11. *Trends Cell Biol.* **24**, 407-415.